Electronic Supplementary Material (ESI) for RSC Advances.

Grafted Iron(III) Ions Significantly Enhance NO_2 Oxidation Rate and Selectivity of TiO_2 for Photocatalytic NOx Abatement

Julia Patzsch,[†] Jacob N. Spencer,[‡] Andrea Folli,[‡] and Jonathan Z. Bloh[*,†]

†*DECHEMA-Forschungsinstitut, Theodor-Heuss-Allee 25, 60486 Frankfurt am Main, Germany*

‡*School of Chemistry, Cardiff University, Main Building, Park Place, Cardiff CF10 3AT, Wales, United Kingdom*

E-mail: bloh@dechema.de

1 Supporting Information

1.1 EPR spectroscopy: *g*-Tensor identification

The resonances at $g = 9.678$, 6, 4.286 and the broad background signal are indicative of high spin Fe(III), ${}^6S_{5/2}$ ground term (5 unpaired electrons), described by the total spin Hamiltonian in Equation 1, sum of electron Zeeman and zero field interactions.

$$\hat{H}(Fe(III)) = \hat{H}_{EZI} + \hat{H}_{ZFI} = \mu_B \boldsymbol{B}^T \boldsymbol{g} \boldsymbol{S} + D\left[\hat{S}_z^2 - \frac{1}{3}S(S+1)\right] + E(\hat{S}_x^2 - \hat{S}_y^2) \qquad (1)$$

In Equation 1, μ_B is the Bohr magneton, $\boldsymbol{B}$ the applied magnetic field, $\boldsymbol{g}$ the g-matrix of the unpaired electrons, $\boldsymbol{S}$ the total spin vector (S_x, S_y, S_z are components of spin along three

mutually perpendicular crystalline axes x, y, and z) and D and E are the zero field splitting parameters, which are induced by distortions of the crystal field in the compound. At least three different ferric crystallographic environments are responsible for the Fe(III) resonances in Fig. 3. The almost isotropic resonance at $g = 4.286$ is often found in strong ($D > h\nu$) low symmetry ($E/D \approx 1/3$) crystal field.[1,2] This resonance arises from the transition within the middle Kramers doublet of the six energy levels ($2S + 1 = 6$ where $S = 5/2$) that at zero field are grouped in three states doubly degenerate (*i.e.* $m_s = \pm 5/2;\ \pm 3/2;\ \pm 1/2$).[1] The upper and lower pairs have strongly anisotropic g values. The three principal values of the diagonalized **g** matrix are 9.678, 0.857, 0.607.[1] Only the first value is visible in the spectrum as the other two are above the upper limit of the magnetic field scanned in the present experiment. The resonance at $g = 6$ corresponds to another ferric crystallographic environment with low symmetry ($E/D = 0$).[1,2] Solution of the spin Hamiltonian for this crystallographic environment provide a g equal to 6 when the magnetic field is perpendicular to S_z and a g equal to 2 when the magnetic field is parallel to S_z.[1] This resonance at $g = 2$ is not readily visible as it is covered by the other signals present at free spin region. However, in a powder one gets all the orientations in the external magnetic field, hence resonances extending from the lowest field, $g = 6$, to the highest field, $g = 2$, with the perpendicular component being statistically more probable than the parallel one. Finally, the broad background signal is produced by crystallographic environments where D and E are both significant and the ratio E/D is in between the limit cases of $E/D = 0$ and $E/D \approx 1/3$. There is no evidence in the spectrum of signals associated with low spin Fe(III), $^2S_{1/2}$ ground term (1 unpaired electron). This species would exhibit an axial $\boldsymbol{g}$ tensor with principal values around 2.23 and 1.93, that are not found in the spectrum in Fig. 3.[2]

1.2 Kinetic analysis of the NOx oxidation performance

The data were either analyzed using Langmuir-Hinshelwood kinetics or, when the reaction rate was found to be linear with the inlet concentration, with first-order kinetics. In both cases, the reaction rates were calculated from the kinetic expressions using the conversion equations for a plug flow type reactor.

$$k^1 = -\frac{ln(c/c0)}{\tau} \tag{2}$$

This yields eqn. 2 for the case of first-order kinetics which was fit to the measured data points using linear regression. For Langmuir-Hinshelwood kinetics, no explicit equation could be obtained. Therefore, the rate law, eqn. 3, was numerically integrated over the reactor volume using Euler-Cauchy algorithm with a step-width of $0.001V$. The resulting value was then fit to the measured data points using non-linear optimization (Levenberg-Marquardt algorithm). Subsequently, first-order rate constants were calculated from eqn. 4.

$$\frac{dc}{dt} = -\frac{k \cdot K \cdot c}{K \cdot c + 1} \tag{3}$$

$$k^1 = k \cdot K \tag{4}$$

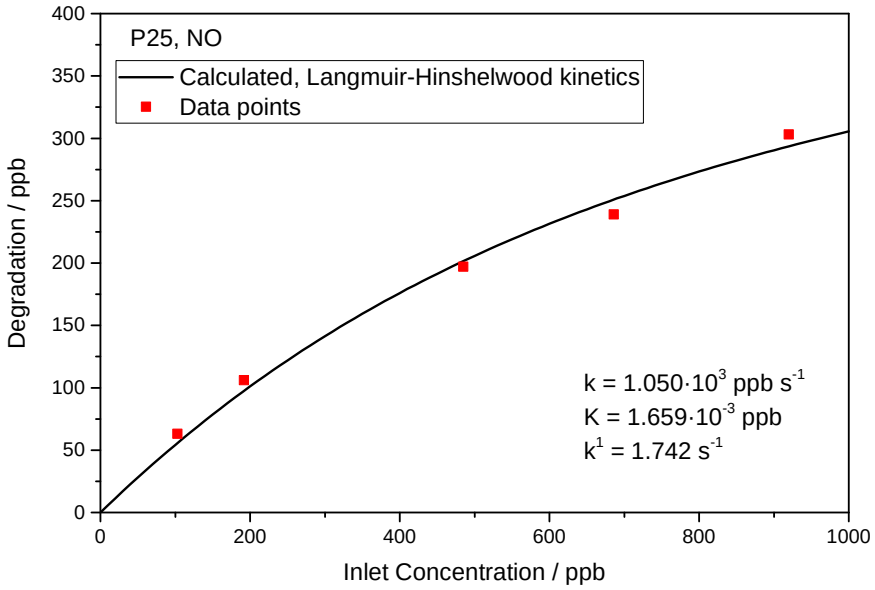

Figure S1: The conversion of NO over illuminated P25 as a function of inlet concentration analyzed using Langmuir-Hinshelwood kinetics.

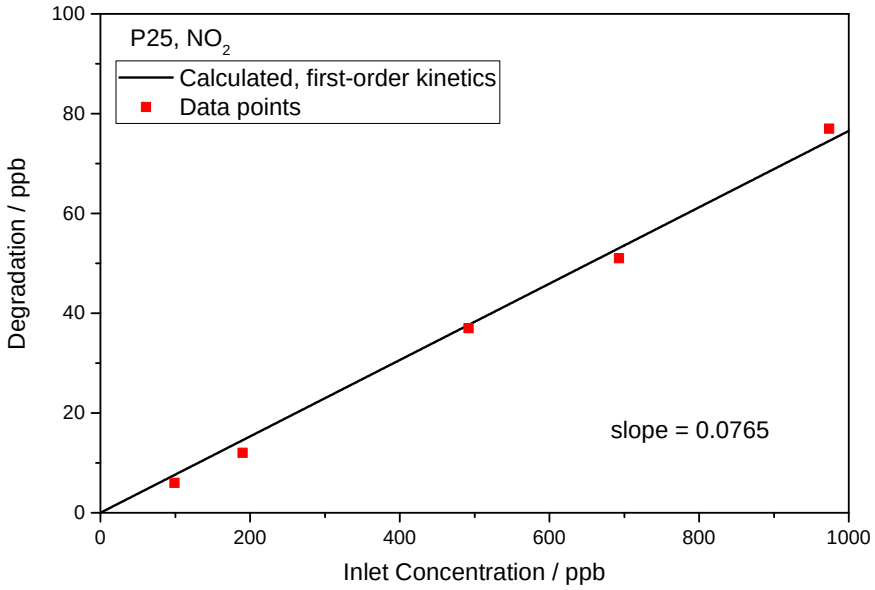

Figure S2: The conversion of NO_2 over illuminated P25 as a function of inlet concentration analyzed using first-order kinetics.

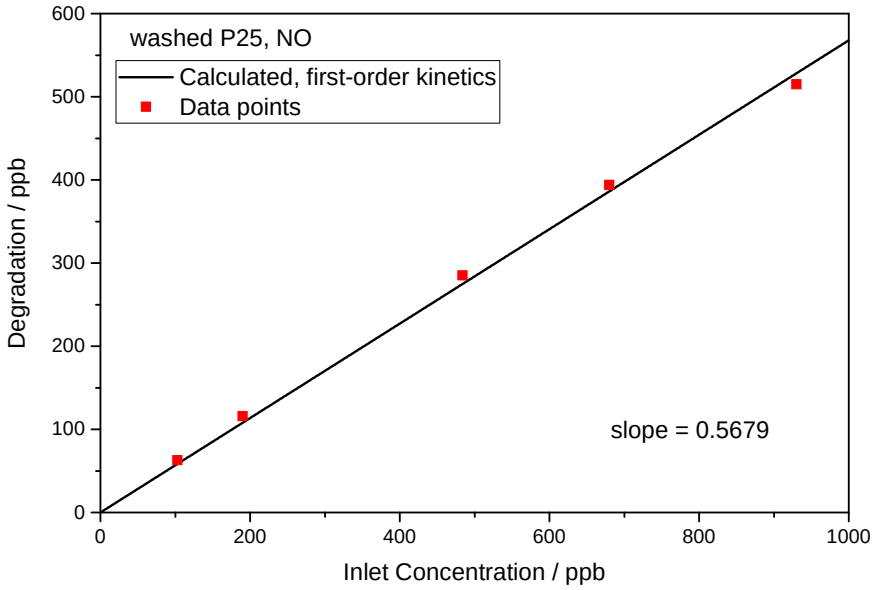

Figure S3: The conversion of NO over illuminated washed P25 as a function of inlet concentration analyzed using first-order kinetics.

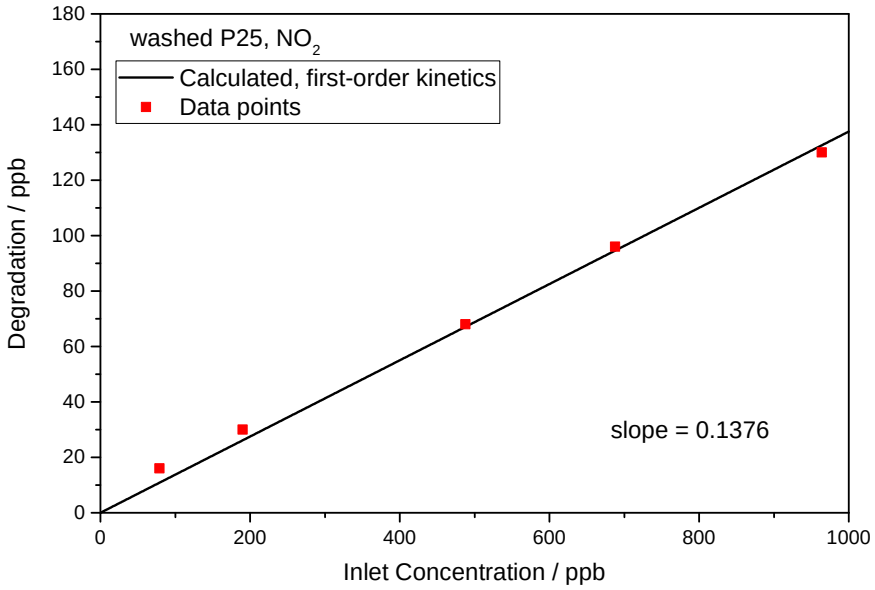

Figure S4: The conversion of NO_2 over illuminated washed P25 as a function of inlet concentration analyzed using first-order kinetics.

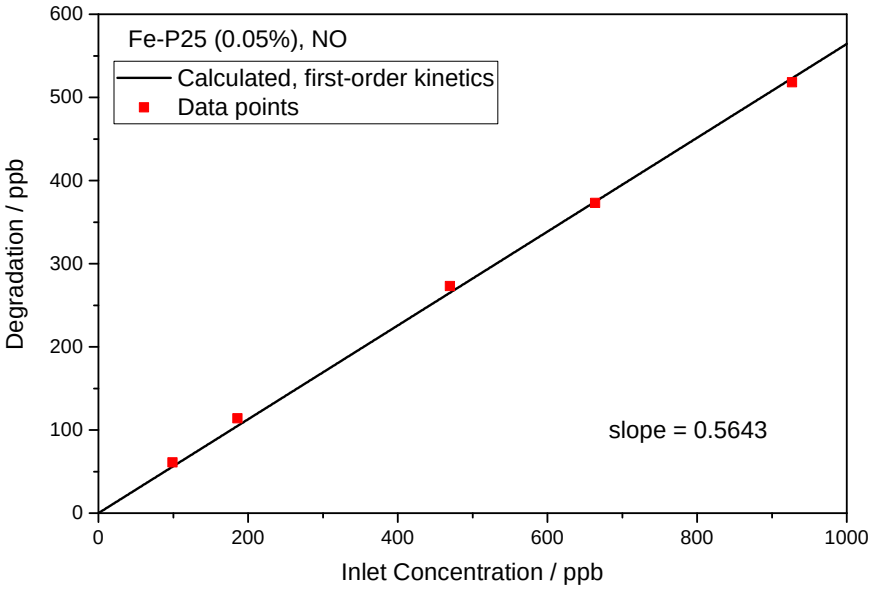

Figure S5: The conversion of NO over illuminated iron-grafted P25 (0.05 at.% Fe) as a function of inlet concentration analyzed using first-order kinetics.

1.3 XPS analysis

A sample grafted with 0.01at.% Fe was subjected to XPS analysis. As seen in Fig. S6, traces of iron might be present (0.1 at.%) but the signals are very low and near the detection limit so any kind of quantitative interpretation is extremely difficult.

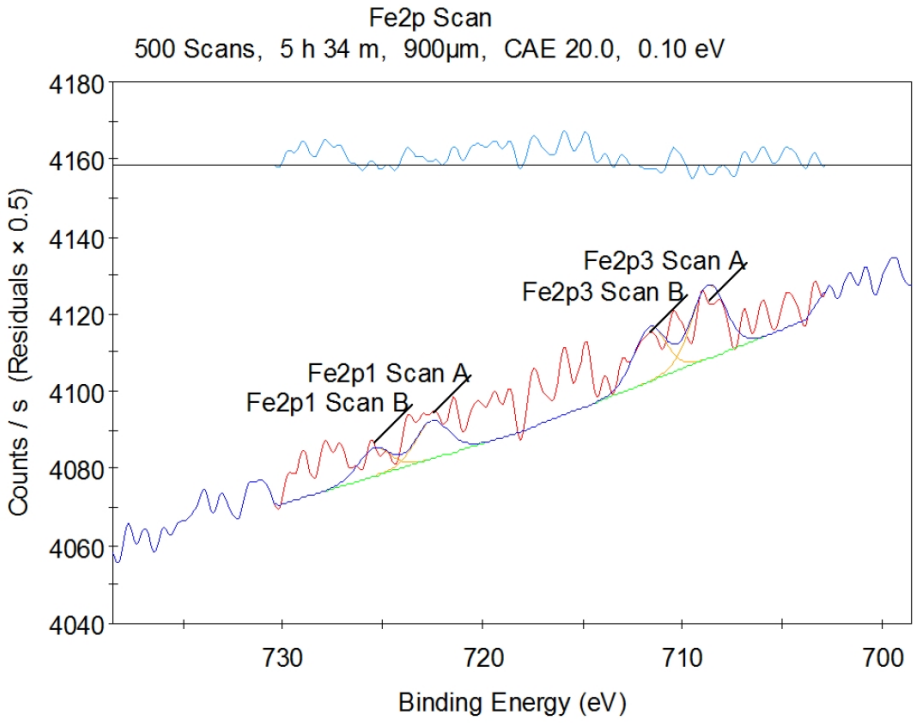

Figure S6: XPS analysis of a sample grafted with 0.01at.% Fe, shown is the binding energy region specific for Fe2p.

1.4 NOx oxidation performance of Mn- oder Cu-grafted P25

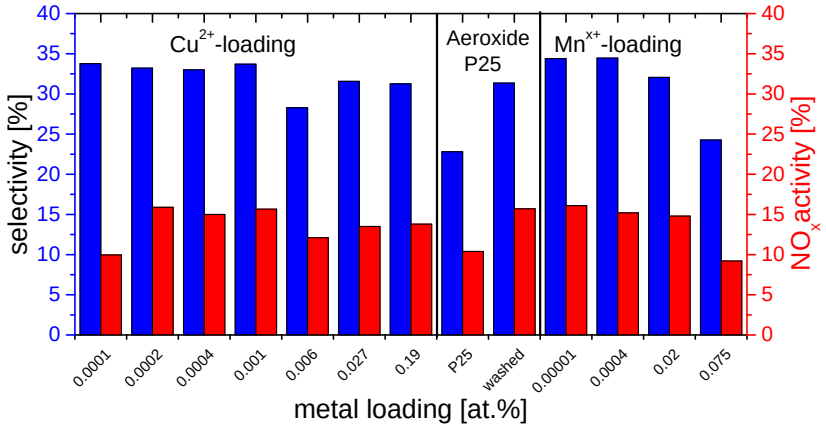

Figure S7: The DeNOx-performance of P25 samples grafted with different amounts of Cu(II) and Mn(II) ions. Displayed are the nitrate selectivity (blue) as well as the NO_x removal rates (red).

1.5 NOx oxidation performance of other commercially available TiO_2 materials grafted with Fe(II) ions

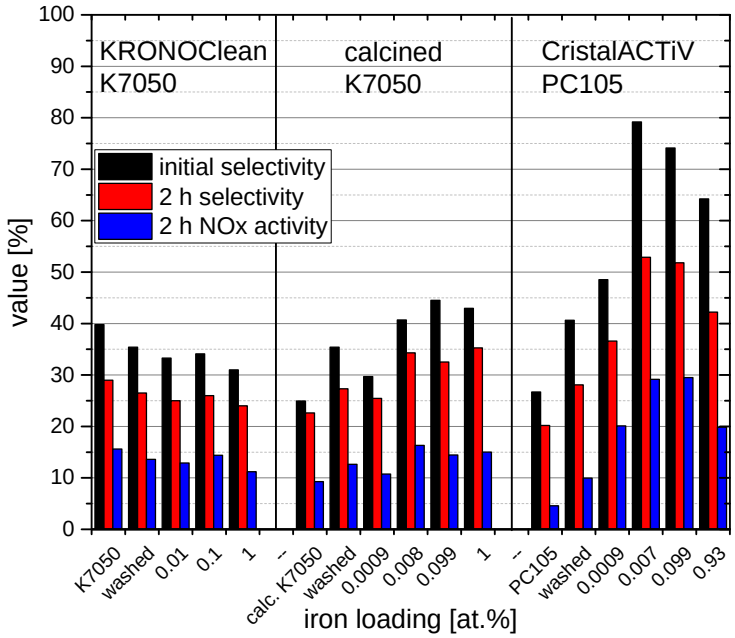

Figure S8: The DeNOx-performance of other TiO_2 materials grafted with different amounts of iron. Displayed are the initial nitrate selectivity (black) as well as the selectivity (red) and NO_x removal rates (blue) after 2 h on stream. The KRONOClean K7050 material is shown before and after calcination at 400 °C for 4 h in air prior to the grafting procedure.

References

(1) Castner Jr., T.; Newell, G.; Holton, W.; Slichter, C. Note on the paramagnetic resonance of iron in glass. *J. Chem. Phys.* **1960**, *32*, 668–673.

(2) Domracheva, N.; Pyataev, A.; Manapov, R.; Gruzdev, M.; Chervonova, U.; Kolker, A. Structural, magnetic and dynamic characterization of liquid crystalline iron(III) Schiff base complexes with asymmetric ligands. *Eur. J. Inorg. Chem.* **2011**, 1219–1229.